

Imperceptible Protection against Style Imitation from Diffusion Models

Namhyuk Ahn^{1,2} Wonhyuk Ahn¹ KiYoon Yoo³ Daesik Kim¹ Seung-Hun Nam¹

¹ NAVER WEBTOON AI ² Inha University ³ Seoul National University
nhahn@inha.ac.kr

Abstract

Recent progress in diffusion models has profoundly enhanced the fidelity of image generation, but it has raised concerns about copyright infringements. While prior methods have introduced adversarial perturbations to prevent style imitation, most are accompanied by the degradation of artworks' visual quality. Recognizing the importance of maintaining this, we introduce a visually improved protection method while preserving its protection capability. To this end, we devise a perceptual map to highlight areas sensitive to human eyes, guided by instance-aware refinement, which refines the protection intensity accordingly. We also introduce a difficulty-aware protection by predicting how difficult the artwork is to protect and dynamically adjusting the intensity based on this. Lastly, we integrate a perceptual constraints bank to further improve the imperceptibility. Results show that our method substantially elevates the quality of the protected image without compromising on protection efficacy.

Introduction

The groundbreaking advancements in large-scale diffusion models have transformed media creation workflows (Rombach et al. 2022; Balaji et al. 2022; Li et al. 2022; Podell et al. 2023; Saharia et al. 2022). These can be further enhanced in usability when integrated with external modules that accept multi-modal inputs (Zhang, Rao, and Agrawala 2023; Li et al. 2023; Mou et al. 2023; Huang et al. 2023; Kim et al. 2023). Such innovations have also been pivotal in the realm of art creation (Ko et al. 2023; Sohn et al. 2023; Ahn et al. 2023). Nevertheless, generative AI, while undoubtedly beneficial, brings concerns about its potential misuse. When someone exploits these to replicate artworks without permission, it introduces significant risks of copyright infringement. This *style imitation* becomes a serious threat to artists (Shan et al. 2023; Xiang 2022).

To counteract style imitation, previous studies have introduced adversarial perturbation (Goodfellow, Shlens, and Szegedy 2014; Madry et al. 2017) to artwork, transforming it into an adversarial example that can resist few-shot generation or personalization methods (Van Le et al. 2023; Liang et al. 2023; Liang and Wu 2023; Ye et al. 2023; Zheng et al. 2023; Salman et al. 2023; Zhao et al. 2023). Specifically, building on the Stable Diffusion (SD) model (Rombach et al. 2022), they iteratively optimize the protected (or perturbed)

image to fool the diffusion models, guided by the gradients from the image encoder or denoising UNet.

While existing studies are effective in preventing style imitation, they do not prioritize the protected image's quality. They leave discernible traces (or artifacts) on the protected images due to the inherent nature of adversarial perturbations. Moreover, we observed that unlike adversarial attacks on classifiers (Luo et al. 2022; Dai et al. 2023), style protection requires more intense and globally dispersed perturbations. Consequently, despite the commendable protection performance, prior works run the risk of severely degrading the original artwork's fidelity, making it less practical for real-world applications. While moderating the strength of protection could mitigate this, it introduces a trade-off, often compromising protection performance and making it challenging to achieve satisfactory results.

To address this, we propose IMPASTO (Figure 1). We design upon the principle of *perception-aware protection*, which focuses on perturbing regions less discernible to humans. While many studies in the adversarial attacks regime limit perturbations to small areas to maximize imperceptibility (Croce and Hein 2019; Dai et al. 2023), they are ineffective for style protection, as personalization methods can leverage references from non-perturbed textures. We instead adopt a *soft restriction* strategy, which protect the entire image but with modulated intensities, relaxing the harsh condition of sparse constraints. To implement this, it is crucial to identify which areas are perceptually more noticeable when perturbations are introduced. For this purpose, we analyze various perceptual maps that are suitable for our task. Then, we propose a method that combines such perceptual maps and refines them in an image-specific manner. Such an *instance-wise refinement* sets itself apart from previous protection methods as it offers a way to strike the optimal balance between imperceptibility and protection performance.

For better imperceptibility, we propose a *difficulty-aware protection* that automatically adjusts the protection strength based on how easily the area can be protected. To achieve this, we compute a *difficulty map*, which predicts the protection difficulty of a given artwork. The difficulty map is then combined with the perceptual map to determine the final protection intensity. Lastly, we introduce a *perceptual constraint bank*, which uses various features to apply perceptual constraints. It may seem unsurprising that a constraint

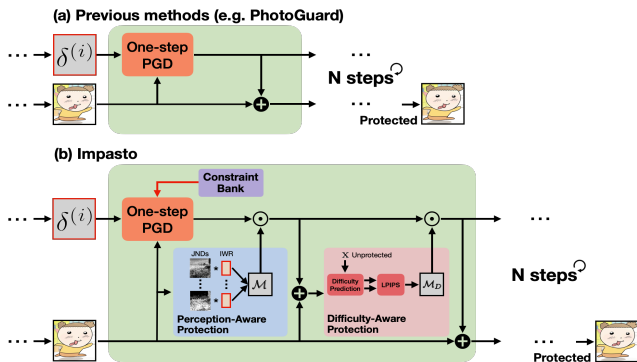


Figure 1: **Model overview.** (a) Previous methods protect image through an iterative process that updates perturbations δ with PGD. (b) On this basis, IMPASTO constructs a perceptual map \mathcal{M} and a difficulty map \mathcal{M}_D to adaptively refine the perturbation for imperceptibility. Additionally, IMPASTO employs a constraint bank in the PGD process to achieve better imperceptibility. Red-bordered boxes indicate trainable parameters. IWR denotes instance-wise refinement.

bank can improve imperceptibility intuitively. However, our study is the first to apply constraints across multiple spaces, improving fidelity without compromising robustness.

To the best of our knowledge, IMPASTO is the **pioneering approach that prioritizes the protected image’s quality** in the style protection task. It achieves robust protection against style imitation and maintains visual fidelity in protected images thus it can significantly improve the trade-off balance between protection efficacy and image quality. Moreover, **IMPASTO is versatile**, enabling its attachment to any existing protection frameworks (Liang et al. 2023; Salman et al. 2023; Van Le et al. 2023; Liang and Wu 2023). IMPASTO also maintains resilience and generalizes well against a range of countermeasures and personalization techniques, performing on par with the baseline methods.

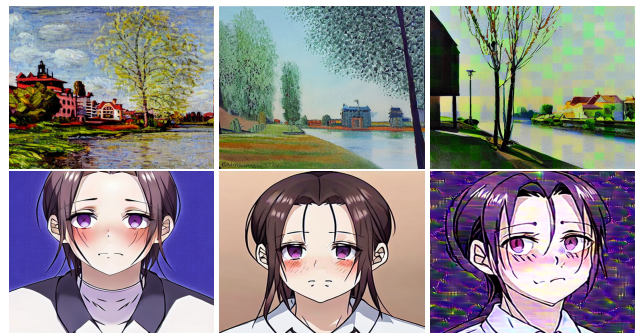
Background

Diffusion Models. These have gain prominence for their capacity to produce high-quality images (Ho, Jain, and Abbeel 2020; Dhariwal and Nichol 2021; Saharia et al. 2022; Nichol et al. 2021; Balaji et al. 2022). In AI-assisted art production, Stable Diffusion (SD) (Rombach et al. 2022) is widely used because of its efficiency. In SD, an input image \mathbf{x} is projected into a latent code via an image encoder \mathcal{E} ; $\mathbf{z} = \mathcal{E}(\mathbf{x})$. A decoder \mathcal{D} reverts the latent code to the image domain; $\mathbf{x}' = \mathcal{D}(\mathbf{z}')$. The diffusion model derives a modified code \mathbf{z}' using external factors y , such as text prompt or other modalities (Zhang, Rao, and Agrawala 2023; Kim et al. 2023). The training objective for SD at timestep t is defined as:

$$\mathcal{L}_{SD} = \mathbb{E}_{\mathbf{z} \sim E(\mathbf{x}), y, \epsilon \sim N(0,1), t} [\|\epsilon - \epsilon_\theta(\mathbf{z}_t, t, c(y))\|_2^2]. \quad (1)$$

Here, a denoising UNet ϵ_θ reconstructs the noised latent code \mathbf{z}_t , given t and a conditioning vector $c(y)$.

Protection Against Style Imitation. Previous methods introduce adversarial perturbations δ to image \mathbf{x} , making pro-



(a) No protect (b) Partial protect (c) Full protect

Figure 2: **Comparison of restriction types.** We compare partial and full protection by fine-tuning diffusion models using protected (or original) images via DreamBooth (Ruiz et al. 2023). For partial protection, perturbations are applied to the center (or facial) region. The results indicate that partial protection is insufficient for style protection, as personalization methods can utilize unprotected areas to learn the artwork’s style. Reference images are shown in Suppl.

ected image $\hat{\mathbf{x}} = \mathbf{x} + \delta$ through projected gradient descent (PGD) (Madry et al. 2017). **1) Encoder-based** methods (Shan et al. 2023; Salman et al. 2023; Ye et al. 2023; Liang and Wu 2023) (e.g. PhotoGuard) update δ under the guidance of the encoder \mathcal{E} . They aim to maximize the distance between the feature of the original and protected image. In practice, many methods minimize the distance between the protected image and target image \mathbf{y} instead:

$$\delta = \underset{\|\delta\|_\infty \leq \eta}{\operatorname{argmin}} \mathcal{L}_\mathcal{E}(\mathbf{x} + \delta, \mathbf{y}), \quad \mathcal{L}_\mathcal{E} = \|\mathcal{E}(\mathbf{x} + \delta) - \mathcal{E}(\mathbf{y})\|_2^2. \quad (2)$$

While L_∞ norm ($\|\delta\|_\infty \leq \eta$; η is a budget) is widely used, GLAZE (Shan et al. 2023) adopts LPIPS (Zhang et al. 2018) and DUAW (Ye et al. 2023) employs SSIM (Wang et al. 2004). **2) Diffusion-based** methods (Van Le et al. 2023; Liang et al. 2023; Salman et al. 2023; Zhao et al. 2023; Liang and Wu 2023) (e.g. AdvDM) update δ under the guidance of UNet, ϵ_θ , maximizing diffusion loss \mathcal{L}_{SD} :

$$\delta = \underset{\|\delta\|_\infty \leq \eta}{\operatorname{argmax}} \mathcal{L}_{SD}(\mathcal{E}(\mathbf{x} + \delta)). \quad (3)$$

Upon this, Anti-DreamBooth (Van Le et al. 2023) integrates DreamBooth training and Mist (Liang and Wu 2023) merges Eq. 2 and 3, enhancing performance and robustness in various scenarios. Since IMPASTO is versatile and can be effortlessly integrated into any existing protection methods, we generalize the style protection as below formulation.

$$\delta = \underset{\|\delta\|_\infty \leq \eta}{\operatorname{argmax}} \mathcal{L}_{SP}(\mathbf{x} + \delta, \mathbf{y}), \quad (4)$$

where $\mathcal{L}_{SP} = -\lambda_\mathcal{E} \mathcal{L}_\mathcal{E}(\mathbf{x} + \delta, \mathbf{y}) + \lambda_{SD} \mathcal{L}_{SD}(\mathcal{E}(\mathbf{x} + \delta))$. Then, we employ PGD to get a protected image $\hat{\mathbf{x}}$. Let $\mathbf{x}^{(0)}$ denote the original image. The protected image of i -th optimization step is generated by a signed gradient ascent with step function sgn and step length α as given by:

$$\mathbf{x}^{(i)} = \Pi_{\mathcal{N}_\eta(\mathbf{x})} \left[\mathbf{x}^{(i-1)} + \alpha \operatorname{sgn}(\nabla_{\mathbf{x}^{(i)}} \mathcal{L}_{SP}(\mathbf{x}^{(i-1)}, \mathbf{y})) \right], \quad (5)$$



Figure 3: **Examples of perceptual maps.** In this study, we use luminance adaptation (LA), contrast masking (CM), contrast sensitivity function (CSF), standard deviation (Stdev), and entropy. **(Left)** Perceptual Map visualization. Darker region corresponds to increased protection intensity. IMPASTO constructs perceptual map \mathcal{M} by spatially averaging these estimations (Average) or an learnable manner (IWR). **(Right)** Perceptual map comparison. We evaluate the protection performance of each perceptual map. Image quality is assessed through DISTS (Ding et al. 2020), and protection performance is evaluated via FID (Heusel et al. 2017). The baseline is trained with Eq. 5 and other models are trained via Eq. 6 with corresponding JNDs.

where $\Pi_{\mathcal{N}_\eta(\mathbf{x})}$ is the projection onto L_∞ neighborhood with radius η . This process is repeated N steps as $\hat{\mathbf{x}} = \mathbf{x}^{(N)}$.

Method

Perception-Aware Protection

Naive sparse restriction. In adversarial attacks, perturbations are often confined to a sparse region to increase imperceptibility (Croce and Hein 2019; Dai et al. 2023). Yet, we observed that they can not sufficiently prevent style imitation. In Figure 2, we compare the protection encompassing the entire image against the one that applies perturbation to facial region only. It is shown that the partial protection cannot protect original artwork against DreamBooth (Ruiz et al. 2023) and we argue that this is because the personalization method can leverage textures from unprotected regions. Overall, sparse restriction may confine the perturbed region too aggressively, thus we relax such assumptions to better align with the style protection task.

Soft restriction. In this study, we instead adopt a soft restriction strategy. It protects the entire image but with varying intensities across different regions. To this end, we introduce a perceptual map, $\mathcal{M} \in \mathbb{R}^d$, where d is the number of pixels of an image. This map reflects the human sensitivity to subtle alterations; a value near 1.0 indicates a region with the highest perceptibility, while a value close to 0.0 signifies a region where changes are hardest to notice. With \mathcal{M} , we define perception-aware protection loss $\mathcal{L}_{\mathcal{PAP}}(\mathbf{x}, \delta, \mathbf{y}, \mathcal{M})$, which use soft restriction-based L_p norm constraint as:

$$\mathcal{L}_{\mathcal{PAP}} = \mathcal{L}_{\mathcal{SP}}(\mathbf{x} + \delta, \mathbf{y}) + \left(\sum_{i=1}^d |\mathcal{M}_i * \delta_i|^p \right)^{1/p}, \quad (6)$$

where $*$ denotes element-wise multiplication. Employing a soft restriction-based L_p norm controls perturbations to be suppressed in regions with high perceptual visibility to humans and amplified in areas with lower visibility. The question now is, how can we determine perceptual sensitivity?

Perceptual map. To build a perceptual map \mathcal{M} in a simple yet effective manner, we investigate the just noticeable difference (JND) concept (Wu, Shi, and Lin 2019) inspired by the human visual system. JND represents the minimum

intensity of stimulus (perturbation in our context) required to produce a noticeable change in visual perception. The intent behind the JND estimation model is to determine this perceptual threshold. Given that the fundamental premise of JND—to quantify human sensitivity to subtle changes—aligns with our objective of perception-aware protection, we focus on analyzing the effectiveness of JNDs in our formulation, and which JND models yield the good results.

To this end, as shown in Figure 3, we compare five widely used JNDs: **1)** luminance adaptation (LM), which considers pixel luminance (Jarsky et al. 2011), **2)** contrast masking (CM), which measures scene complexity by luminance contrast (Legge and Foley 1980; Wu et al. 2013a), **3)** contrast sensitivity function (CSF), which utilizes frequency signals (Wei and Ngan 2009), **4)** standard deviation (Stdev), which measures spatial structure with patch-wise statistics, and **5)** entropy, which computes complexity with patch-wise entropy. More details are described in Suppl.

In our observation, most JND models fit surprisingly well with soft restriction (Figure 3, right). Consequently, we employ a JND-based perceptual maps, considering its simplicity and effectiveness. Note that among JNDs we used, LA and CM emerge as superior in the quality-protection trade-off. However, these results are the *average scores* across a dataset and we note that some artworks exhibit better trade-off with other JNDs. Especially, since artworks have diverse styles, the best combinations can differ; for example, in Figure 3 (left), Stdev and entropy are best for top image while bottom image shows a preference for CM and CSF. Moreover, in practical scenarios, users who protect their artwork are solely concerned with their specific pieces, not the average scores. Thus, it is crucial to ensure that the protection method is effectively applied to *every individual artwork*.

We therefore apply all the JNDs simultaneously to create the perceptual map, since relying on a single JND could result in decreased performance for some artworks. Formally, for an artwork \mathbf{x} requiring protection, we initially generate a corresponding perceptual map \mathcal{M} with a collection of JNDs, $\mathbf{M} = \{M^1, \dots, M^K\}$, where K is the number of JNDs. To integrate multiple JNDs, the simplest method involves using a spatial average: $\mathcal{M} = \frac{1}{K} \sum_{k=1}^K M^k$.

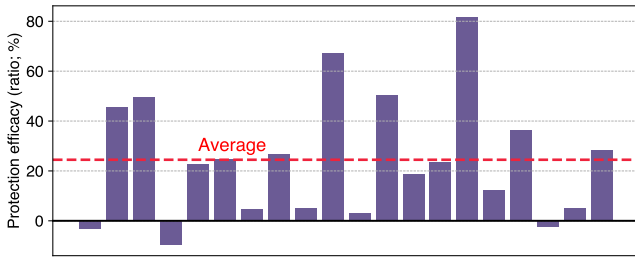


Figure 4: **Protection difficulty.** We present the protection efficacy of PhotoGuard (Salman et al. 2023) across 20 artworks (x-axis). Notably, the level of style protection varies widely between artworks, thus the average score (red dashed line) is less meaningful to users who protect their artwork.

Instance-wise refinement. Although the above method is more effective in many scenarios than the single JND, applying a uniform averaged map across *all artworks* may still be suboptimal for some artworks. Moreover, the optimal perceptual map corresponding to an artwork varies depending on both artwork’s structure and the applied protective perturbations. Even for identical artwork, the detectability of perturbations is affected by changing these as human sensitivity varies with distortion type (Dodge and Karam 2017). Considering these, we propose an instance-wise refinement (IWR), customizing the perceptual map \mathcal{M} for each artwork. During optimization steps, the perceptual map is refined through a weighted sum: $\mathcal{M}(\omega) = \sum_{k=1}^K \text{softmax}(\omega)^k * M^k$, where ω is a set of learnable parameters that adjust the contributions of each JND to \mathcal{M} . The refinement parameters ω is optimized using the objective function below:

$$\mathcal{L}_{\mathcal{M}} = \|\mathcal{L}_{SP}(\mathbf{x} + \mathcal{M}' \odot \delta) - \mathcal{L}_{SP}(\mathbf{x} + \mathcal{M}(\omega) \odot \delta)\|_2^2 + \left(\sum_{i=1}^d |\mathcal{M}(\omega)_i * \delta_i|^p \right)^{\frac{1}{p}}, \quad (7)$$

with \mathcal{M}' being the initial perceptual map before the refinement steps. In Eq. 7, the former term enforces the consistency of the refined perceptual map \mathcal{M} with the initial map \mathcal{M}' by minimizing the discrepancy in protection loss between them. The latter term enhances the perception-aware protection for a given specific image. As shown in Figure 3, instance-wise refinement (IWR) has a pronounced effect as compared to the naive averaging, better capturing the nuances of image-specific perceptual sensitivity.

Difficulty-Aware Protection

We observed that the difficulty of protection varies across images (or artworks); some images are protected properly with low protection strength, while others require higher strength to achieve the same protection level. Figure 4 shows the protection efficacy of PhotoGuard (Salman et al. 2023) in 20 artworks. The score is calculated as $(\text{FID}_{\text{protected}} - \text{FID}_{\text{unprotected}}) / \text{FID}_{\text{unprotected}}$, with a higher value indicating better protection efficacy. Surprisingly, the protection efficacy varies greatly across artworks. Moreover, some artworks show no difference between unprotected and protected cases. It implies that, for actual users, the *average*

Algorithm 1: Optimization of IMPASTO

Data: Image \mathbf{x} , target image \mathbf{y} , perceptual maps \mathbf{M}
Result: Protected image $\hat{\mathbf{x}}$
Init $\mathbf{x}^{(0)} \leftarrow \mathbf{x}$, $\mathcal{M}' \leftarrow \frac{1}{K} \sum_{k=1}^K M^k$, $\omega \leftarrow \frac{1}{K} \cdot \mathbf{1}^K$
for $i = 1$ **to** N **do**
 $\delta^{(i)} \leftarrow \alpha \text{sgn}(\nabla_{\delta^{(i)}} \mathcal{L}(\mathbf{x}^{(i-1)}, \delta^{(i-1)}, \mathbf{y}, \mathcal{M}))$
 $\mathbf{x}^{(i)} \leftarrow \Pi_{\mathcal{N}_\eta(\mathbf{x})}(\mathbf{x}^{(i-1)} + \delta^{(i)} \odot \mathcal{M}(\omega) \odot \mathcal{M}_D)$
 if $i \bmod P == 0$ **then**
 /* Instance-wise refinement */
 $\omega \leftarrow \omega - \nabla_\omega \mathcal{L}_{\mathcal{M}}(\mathbf{x}, \delta^{(i)}, \mathbf{y}, \mathcal{M}', \mathcal{M}(\omega))$
 /* Difficulty-aware protection */
 $\mathcal{M}_D = \text{DAP}(\mathbf{x}, \mathbf{x}^{(i)})$
 end
end
 $\hat{\mathbf{x}} \leftarrow \mathbf{x} + \delta^{(N)} \odot \mathcal{M}(\omega) \odot \mathcal{M}_D$

score might be a meaningless metric. So why does the level of protection differ between artworks? This question may tie into the learning dynamics of personalization methods, which are still unclear and require further investigation.

Nevertheless, we understand that the protection performance differs between artworks, so in practice, we can adjust the protection strength accordingly when we know the *difficulty*. The most straightforward way to predict the difficulty is to perform protection, personalize the protected/unprotected images with DreamBooth (Ruiz et al. 2023), and evaluate protection efficacy as done in Figure 4. While effective, this is extremely time-consuming as it requires two personalization stages (for protected and unprotected images).

To predict difficulty more practically, we approximate the above procedure. At the i -th perturbation optimization step, we obtain an intermediate protected image as $\mathbf{x}^{(i)} = \mathbf{x} + \delta^{(i)}$. Then, along with the unprotected image \mathbf{x} , we create a difficulty map \mathcal{M}_D with a difficulty-aware protection function; $\mathcal{M}_D = \text{DAP}(\mathbf{x}, \mathbf{x}^{(i)})$. This function is defined as follows:

$$\text{DAP}(\mathbf{x}, \mathbf{x}^{(i)}) = \text{LPIPS}(\text{DP}(\mathbf{x}), \text{DP}(\mathbf{x}^{(i)})), \quad (8)$$

where $\text{LPIPS}(\cdot)$ denotes the spatial LPIPS distance (Zhang et al. 2018). In the difficulty prediction module, denoted as $\text{DP}(\cdot)$, an input image \mathbf{x} (or the unprotected image $\mathbf{x}^{(i)}$ but omitting the superscript for clarity) is passed through an encoder \mathcal{E} to obtain the latent code \mathbf{z} . A forward diffusion process is then applied for t timestep, followed by a reverse diffusion process using the denoising UNet, ϵ_θ . Finally, the decoder \mathcal{D} projects this back to the image space:

$$\text{DP}(\mathbf{x}) = \mathcal{D}(\tilde{\mathbf{z}}_0), \quad \text{where} \quad (9)$$

$$\tilde{\mathbf{z}}_0 = \text{Reverse}(\mathbf{z}_t; \epsilon_\theta), \quad \mathbf{z}_t = \text{Forward}(\mathcal{E}(\mathbf{x}), t),$$

where $\text{Forward}(\cdot)$ and $\text{Reverse}(\cdot)$ denote the forward and reverse diffusion processes, respectively. We limit the diffusion process to t timestep to reduce major structural changes.

The difficulty and the perceptual map are used to compute the protection image as: $\hat{\mathbf{x}} = \mathbf{x} + \mathcal{M} \odot \mathcal{M}_D \odot \delta$. In this approximated approach, we can replace the difficulty prediction involving full personalization with the diffusion process

Table 1: **Quantitative comparison** of protection methods w/ and w/o IMPASTO, both selected for their comparable protection performance. IMPASTO markedly elevates the protected images’ quality while maintaining protection efficacy.

Dataset	Method	Protected Image Quality			Protection Performance		
		DISTS (\downarrow)	PicAPP (\downarrow)	TOPIQ (\uparrow)	NIQE (\uparrow)	BRISQUE (\uparrow)	FID (\uparrow)
Painting	PhotoGuard	0.181 (+0.000)	0.364 (+0.000)	0.896 (+0.000)	4.306	20.99	277.6
	+ IMPASTO	0.158 (+0.023)	0.285 (+0.079)	0.914 (+0.018)	4.342	18.57	281.0
	AdvDM	0.167 (+0.000)	0.730 (+0.000)	0.846 (+0.000)	3.761	12.45	269.0
	+ IMPASTO	0.135 (+0.032)	0.360 (+0.370)	0.893 (+0.047)	4.011	13.77	269.2
Cartoon	PhotoGuard	0.249 (+0.000)	0.782 (+0.000)	0.797 (+0.000)	5.037	10.19	155.9
	+ IMPASTO	0.206 (+0.043)	0.706 (+0.076)	0.888 (+0.091)	5.620	11.46	157.7
	AdvDM	0.241 (+0.000)	0.776 (+0.000)	0.775 (+0.000)	4.802	10.95	153.5
	+ IMPASTO	0.231 (+0.010)	0.706 (+0.070)	0.888 (+0.113)	5.620	11.46	155.6

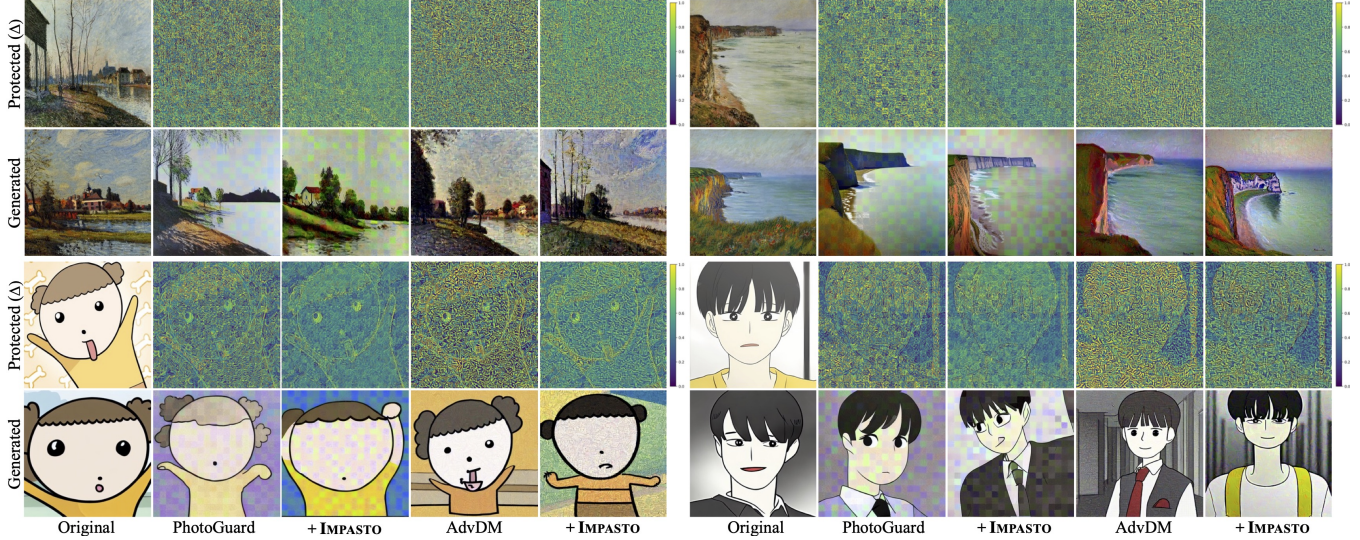


Figure 5: **Qualitative comparison.** We visualize the difference map (Δ) between the protected and unprotected images. Yellowish color indicates different regions and bluish color show similar pixels. While maintaining comparable style protection efficacy (artifacts in the generated results), IMPASTO significantly enhances the quality of the protected images.

and LPIPS computation. While full prediction is optimal, we make this approximation to balance practicality. We observe that images with our difficulty-aware protection performed robustly even without the personalization process.

Perceptual Constraint Bank

To further enhance the imperceptibility, we employ a bank of perceptual constraints across multiple feature spaces:

Masked LPIPS. LPIPS (Zhang et al. 2018) is a widely used constraint. Our approach distinguishes itself by applying a *masked* LPIPS constraint, modulating the LPIPS influence using a perceptual map \mathcal{M} . Let ϕ_l be a l -th layer of the LPIPS network, with a corresponding feature map resolution d_l , the masked LPIPS is calculated as:

$$\mathcal{L}_{\mathcal{L}} = \sum_l \frac{1}{d_l} \sum_{i=1}^{d_l} \mathcal{M}_i * \|w_l * (\phi_l(\mathbf{x})_i - \phi_l(\mathbf{x} + \delta)_i)\|_2^2, \quad (10)$$

where w_l is the channel-wise scale parameters. By focusing on perceptually significant regions with a mask, IMPASTO can achieve better protection performance.

Masked low-pass. We also apply a pixel-domain constraint that focuses on the low-frequency components, inspired by Luo et al. (2022). The loss function is as:

$$\mathcal{L}_{\mathcal{LP}} = \frac{1}{d} \sum_{i=1}^d \mathcal{M}_i * \|\text{LP}(\mathbf{x})_i - \text{LP}(\mathbf{x} + \delta)_i\|_2^2, \quad (11)$$

where $\text{LP}(\mathbf{x})$ is the low-frequency component of image \mathbf{x} (please refer to Suppl. for more details). This constraint mimics observing a painting from a distance, where perturbations in smooth regions are perceptible, while detailed textures hide these until we closely inspect the artwork.

CLIP. We leverage CLIP (Radford et al. 2021) which benefits from training on a vast and varied dataset of image-text pairs. With the prompt $C = \text{“Noise-free image”}$, the CLIP constraint aims to maximize the feature distance between the protected image and the descriptive prompt.

$$\mathcal{L}_{\mathcal{C}} = -\cos(\text{CLIP}_I(\mathbf{x} + \delta), \text{CLIP}_T(C)), \quad (12)$$

where $\text{CLIP}_I, \text{CLIP}_T$ are image and text encoders. The final protection loss, $\mathcal{L}(\mathbf{x}^{(i)}, \delta, \mathbf{y}, \mathcal{M})$ combines all the losses,

Table 2: **Component analysis.** PAP: perception-aware protection. w/o JND: initialize M with random masks, not from JNDs. w/o Mask: Constraints without a perceptual map. DAP: difficulty-aware protection. Base*: PhotoGuard with equal protection strength. Base**: PhotoGuard with a similar protection performance (lower protection strength).

Method	Image Quality		Protection Performance	
	DISTS (\downarrow)	TOPIQ (\uparrow)	NIQE (\uparrow)	FID (\uparrow)
Base*	0.212	0.845	4.387	299.1
+ PAP	0.171	0.890	4.253	286.8
w/o JND	0.170	0.892	4.399	278.1
+ LPIPS	0.163	0.910	4.369	280.4
+ Low-pass	0.163	0.911	4.376	277.5
w/o Mask	0.163	0.911	4.142	272.6
+ CLIP	0.159	0.912	4.479	279.2
+ DAP	0.157	0.913	4.342	281.0
Base**	0.181	0.896	4.041	277.6

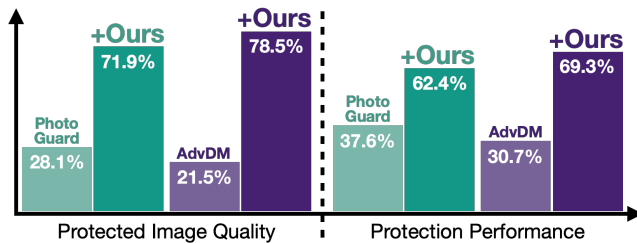


Figure 6: **User preference study** (via A/B test) of PhotoGuard and AdvDM with and without IMPASTO.

weighted by their respective λ s as:

$$\mathcal{L} = \mathcal{L}_{PAP} + \lambda_L \mathcal{L}_L + \lambda_{LP} \mathcal{L}_{LP} + \lambda_C \mathcal{L}_C. \quad (13)$$

Algorithm 1 overviews the protection process of IMPASTO. It is designed to be versatile, allowing the integration of existing protection frameworks. Such adaptability will be discussed in the next section as well as in Suppl.

Experiment

Datasets. We utilize two art domain datasets: painting and cartoon. The painting dataset is curated from WikiArt (Tan et al. 2018) with a selection of 15 artists, 10 works per artist. The cartoon dataset is a collection of 15 cartoons with 10 cartoon face images. Further details are in Suppl.

Measure. We use DISTS (Ding et al. 2020), PieAPP (Prashnani et al. 2018) and TOPIQ (Chen et al. 2023) to assess protected image quality. Protection score is measured via NIQE (Mittal, Soundararajan, and Bovik 2012), BRISQUE (Mittal, Moorthy, and Bovik 2011), and FID (Heusel et al. 2017). For protection metrics, worse scores indicate more effective protection.

Baseline. IMPASTO can be integrated into any existing protection methods. Hence, we adopt IMPASTO into PhotoGuard (Salman et al. 2023) and AdvDM (Liang et al. 2023). In Suppl, applications to Mist (Liang and Wu 2023) and Anti-DreamBooth (Van Le et al. 2023) are also presented.

Table 3: **Perception-aware protection.** The efficacy of JNDs (LA and CM as they show best results) is presented along with an averaged perceptual map and with IWR. IWR[†]: IWR is conducted before optimization.

Method	Image Quality		Protection Performance	
	DISTS (\downarrow)	TOPIQ (\uparrow)	NIQE (\uparrow)	FID (\uparrow)
Baseline	0.212	0.845	4.387	299.1
LA	0.175	0.879	4.298	284.7
CM	0.169	0.882	3.986	280.8
Average	0.170	0.891	3.971	277.9
IWR [†]	0.171	0.894	4.016	282.5
IWR	0.171	0.890	4.306	286.8

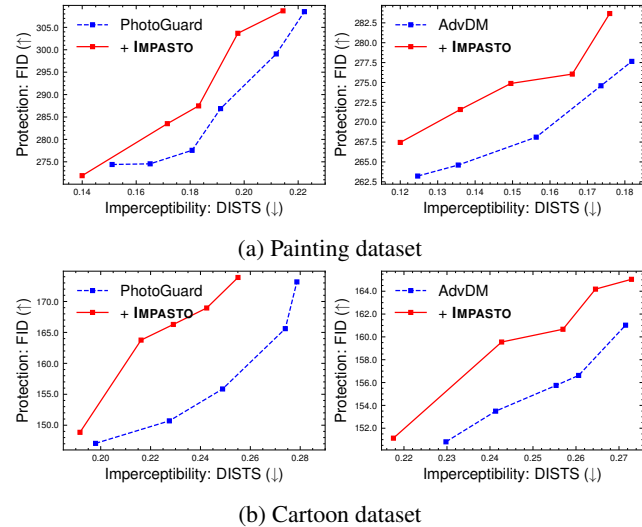


Figure 7: **Style protection comparison.** Protection performance is evaluated with FID and imperceptibility via DISTS. Adaptation of IMPASTO to both PhotoGuard and AdvDM ensures superior performance.

Model Comparison

Table 1 presents a comparison of image quality under a comparable protection performance of the models with and without IMPASTO. Across all the scenarios, IMPASTO substantially enhances the fidelity of the protected images. Figure 5 also supports the superior efficacy of IMPASTO; it successfully minimizes artifacts, in contrast to baselines that leave discernible traces on the artwork. User evaluation further confirms the effectiveness of IMPASTO (Figure 6).

Varying strengths. As demonstrated in Figure 7, we manipulate the protection strengths (budget) to delineate an imperceptibility-protection trade-off curve. On both painting and cartoon datasets, employing IMPASTO into the baselines considerably improves the trade-off dynamics.

Model Analysis

Ablation study. As shown in Table 2, the perception-aware protection (PAP) markedly improves image fidelity over Photoguard (Base*), albeit with a slight reduction in protection efficacy. However, compared to Photoguard with lower

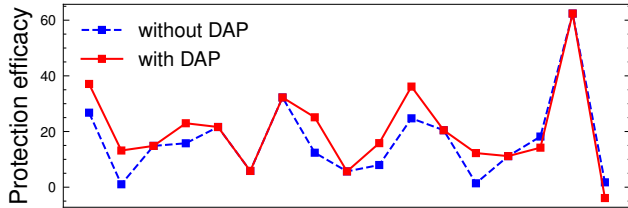


Figure 8: **Difficulty-aware protection.** We compare on the Cartoon dataset with and without the difficulty-aware protection (DAP). Higher values indicates better protection.

strength (Base**), PAP achieves better preservation of protection performance with enhanced image quality. We observed that when \mathcal{M} is formed from a random mask, not JND, (w/o JND), the protection performance is degraded. Employing a constraint bank significantly improves image quality with comparable protection scores to Photoguard (Base**). The omission of the perceptual map \mathcal{M} in the constraints (w/o Mask) leads to a decline in protection performance, akin to the observations in the PAP case. The difficulty-aware protection (DAP) also enhances both image quality and protection efficacy (FID).

Perceptual map. We analyze the perception-aware protection in Table 3. LA and CM enhance the protected image’s fidelity but at the cost of compromising protection performance. Multiple JNDs through averaging leads to better image quality, but it also reduces the protection performance. We speculate that such a straightforward averaging method may not adequately capture the unique structural elements of the image, resulting in overly smooth perturbations that could weaken the protection performance. On the other hand, IWR enhances all protection scores while preserving satisfactory image quality, as it can adapt to the specific textures and structures of a given artwork. It’s noteworthy that applying IWR prior to perturbation optimization (IWR[†]), where it does not consider the perturbations, slightly diminishes protection performance, accentuating the importance of modeling the interplay between artwork and applied perturbation to finalization mask \mathcal{M} .

Difficulty-aware protection. In Figure 8, we demonstrate the change in protection performance with and without difficulty-aware protection (DAP). This method applies stronger intensity in cases of higher protection difficulty and vice versa, leading to a more balanced protection trend.

Countermeasures. To analyze the robustness of IMPASTO, we conduct countermeasure experiments with JPEG compression ($q = 40$), Gaussian blur (3×3 kernel, $\sigma = 0.02$), and Gaussian noise ($\sigma = 0.02$). Results indicate a performance degradation of all protection methods when these countermeasures are applied, as they tend to remove the protective perturbations (Figure 9). Nonetheless, IMPASTO demonstrates comparable robustness against such countermeasures. For the blur effect, there is a slight performance degradation with IMPASTO, as subtle perturbations are particularly weakened to this; we also observed that baseline with low-budget protection is also vulnerable to blur. How-

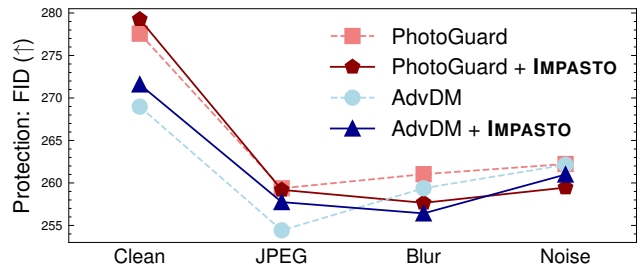


Figure 9: **Robustness evaluation.** Methods with IMPASTO exhibit comparable protection performance to baselines.

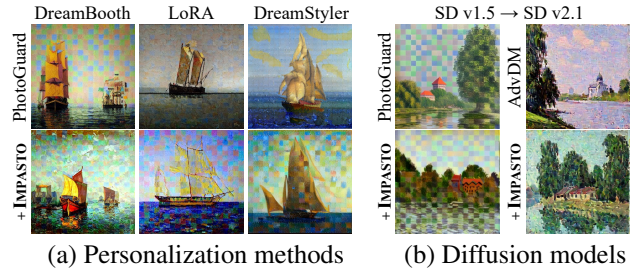


Figure 10: **Generalization.** IMPASTO does not impede baselines’ generalization abilities on (a) different personalization methods; DreamBooth, LoRA, and DreamStyler or (b) model black-box scenario; SD v1.5 \rightarrow v2.1.

ever, the blurring effect also renders the artwork less plausible, making it an impractical choice for malicious users.

Black-box scenario. We broaden the evaluation when applied to other personalization methods. We adopt LoRA (Hu et al. 2021), a standard personalization method, and DreamStyler (Ahn et al. 2023), known for its effectiveness in style adaptation. As shown in Figure 10a, IMPASTO maintains robust protection effectiveness. In style protection, generalization robustness against unknown models is also a crucial aspect. To examine this, we compare by optimizing on SD v1.5 and testing on SD v2.1. As illustrated in Figure 10b, IMPASTO successfully preserves the robustness of PhotoGuard and AdvDM. Overall, in both facets of the black-box scenario; unknown personalization methods and diffusion models, IMPASTO not only maintains the generalization ability but also effectively improves protection images’ quality.

Conclusion

We proposed IMPASTO to prevent style imitation in a perceptual orientation. With perceptual and difficulty-aware protections as well as perceptual constraint bank, IMPASTO markedly improves the quality of the protected images of the baseline protection frameworks.

Limitations. All the current protections mostly adopt adversarial perturbations, which can hamper usability due to the extensive time required for the optimization. Even accessible software (Shan et al. 2023) takes 30-60 mins to protect a 512^2 image on CPU. Addressing this time constraint is a challenge that future research should aim to overcome.

References

- Ahn, N.; Lee, J.; Lee, C.; Kim, K.; Kim, D.; Nam, S.-H.; and Hong, K. 2023. DreamStyler: Paint by Style Inversion with Text-to-Image Diffusion Models. *arXiv preprint arXiv:2309.06933*.
- Balaji, Y.; Nah, S.; Huang, X.; Vahdat, A.; Song, J.; Kreis, K.; Aittala, M.; Aila, T.; Laine, S.; Catanzaro, B.; et al. 2022. ediffi: Text-to-image diffusion models with an ensemble of expert denoisers. *arXiv preprint arXiv:2211.01324*.
- Cao, Q.; Shen, L.; Xie, W.; Parkhi, O. M.; and Zisserman, A. 2018. Vggface2: A dataset for recognising faces across pose and age. In *2018 13th IEEE international conference on automatic face & gesture recognition (FG 2018)*, 67–74. IEEE.
- Chen, C.; Mo, J.; Hou, J.; Wu, H.; Liao, L.; Sun, W.; Yan, Q.; and Lin, W. 2023. TOPIQ: A Top-down Approach from Semantics to Distortions for Image Quality Assessment. *arXiv preprint arXiv:2308.03060*.
- Chou, C.-H.; and Li, Y.-C. 1995. A perceptually tuned sub-band image coder based on the measure of just-noticeable-distortion profile. *IEEE Transactions on circuits and systems for video technology*, 5(6): 467–476.
- Croce, F.; and Hein, M. 2019. Sparse and imperceptible adversarial attacks. In *Proceedings of the IEEE/CVF international conference on computer vision*, 4724–4732.
- Dai, Z.; Liu, S.; Li, Q.; and Tang, K. 2023. Saliency Attack: Towards Imperceptible Black-box Adversarial Attack. *ACM Transactions on Intelligent Systems and Technology*, 14(3): 1–20.
- Damera-Venkata, N.; Kite, T. D.; Geisler, W. S.; Evans, B. L.; and Bovik, A. C. 2000. Image quality assessment based on a degradation model. *IEEE transactions on image processing*, 9(4): 636–650.
- Dhariwal, P.; and Nichol, A. 2021. Diffusion models beat gans on image synthesis. *Advances in neural information processing systems*, 34: 8780–8794.
- Ding, K.; Ma, K.; Wang, S.; and Simoncelli, E. P. 2020. Image quality assessment: Unifying structure and texture similarity. *IEEE transactions on pattern analysis and machine intelligence*, 44(5): 2567–2581.
- Dodge, S.; and Karam, L. 2017. A study and comparison of human and deep learning recognition performance under visual distortions. In *2017 26th international conference on computer communication and networks (ICCCN)*, 1–7. IEEE.
- Goodfellow, I. J.; Shlens, J.; and Szegedy, C. 2014. Explaining and harnessing adversarial examples. *arXiv preprint arXiv:1412.6572*.
- Guo, C.; Frank, J. S.; and Weinberger, K. Q. 2018. Low frequency adversarial perturbation. *arXiv preprint arXiv:1809.08758*.
- Heusel, M.; Ramsauer, H.; Unterthiner, T.; Nessler, B.; and Hochreiter, S. 2017. Gans trained by a two time-scale update rule converge to a local nash equilibrium. *Advances in neural information processing systems*, 30.
- Ho, J.; Jain, A.; and Abbeel, P. 2020. Denoising diffusion probabilistic models. *Advances in neural information processing systems*, 33: 6840–6851.
- Hu, E. J.; Shen, Y.; Wallis, P.; Allen-Zhu, Z.; Li, Y.; Wang, S.; Wang, L.; and Chen, W. 2021. Lora: Low-rank adaptation of large language models. *arXiv preprint arXiv:2106.09685*.
- Huang, L.; Chen, D.; Liu, Y.; Shen, Y.; Zhao, D.; and Zhou, J. 2023. Composer: Creative and controllable image synthesis with composable conditions. *arXiv preprint arXiv:2302.09778*.
- Jarsky, T.; Cembrowski, M.; Logan, S. M.; Kath, W. L.; Riecke, H.; Demb, J. B.; and Singer, J. H. 2011. A synaptic mechanism for retinal adaptation to luminance and contrast. *Journal of Neuroscience*, 31(30): 11003–11015.
- Karras, T.; Aila, T.; Laine, S.; and Lehtinen, J. 2017. Progressive growing of gans for improved quality, stability, and variation. *arXiv preprint arXiv:1710.10196*.
- Kim, S.; Lee, J.; Hong, K.; Kim, D.; and Ahn, N. 2023. DiffBlender: Scalable and Composable Multimodal Text-to-Image Diffusion Models. *arXiv preprint arXiv:2305.15194*.
- Ko, H.-K.; Park, G.; Jeon, H.; Jo, J.; Kim, J.; and Seo, J. 2023. Large-scale text-to-image generation models for visual artists’ creative works. In *Proceedings of the 28th International Conference on Intelligent User Interfaces*, 919–933.
- Krizhevsky, A.; Sutskever, I.; and Hinton, G. E. 2012. Imagenet classification with deep convolutional neural networks. *Advances in neural information processing systems*, 25.
- Larson, E. C.; and Chandler, D. M. 2010. Most apparent distortion: full-reference image quality assessment and the role of strategy. *Journal of electronic imaging*, 19(1): 011006–011006.
- Legge, G. E.; and Foley, J. M. 1980. Contrast masking in human vision. *Josa*, 70(12): 1458–1471.
- Li, W.; Xu, X.; Xiao, X.; Liu, J.; Yang, H.; Li, G.; Wang, Z.; Feng, Z.; She, Q.; Lyu, Y.; et al. 2022. Upainting: Unified text-to-image diffusion generation with cross-modal guidance. *arXiv preprint arXiv:2210.16031*.
- Li, Y.; Liu, H.; Wu, Q.; Mu, F.; Yang, J.; Gao, J.; Li, C.; and Lee, Y. J. 2023. Gligen: Open-set grounded text-to-image generation. In *Proceedings of the IEEE/CVF Conference on Computer Vision and Pattern Recognition*, 22511–22521.
- Liang, C.; and Wu, X. 2023. Mist: Towards Improved Adversarial Examples for Diffusion Models. *arXiv preprint arXiv:2305.12683*.
- Liang, C.; Wu, X.; Hua, Y.; Zhang, J.; Xue, Y.; Song, T.; Xue, Z.; Ma, R.; and Guan, H. 2023. Adversarial example does good: preventing painting imitation from diffusion models via adversarial examples. In *Proceedings of the 40th International Conference on Machine Learning*, 20763–20786.
- Luo, B.; Liu, Y.; Wei, L.; and Xu, Q. 2018. Towards imperceptible and robust adversarial example attacks against neural networks. In *Proceedings of the AAAI conference on artificial intelligence*, volume 32.

- Luo, C.; Lin, Q.; Xie, W.; Wu, B.; Xie, J.; and Shen, L. 2022. Frequency-driven imperceptible adversarial attack on semantic similarity. In *Proceedings of the IEEE/CVF Conference on Computer Vision and Pattern Recognition*, 15315–15324.
- Madry, A.; Makelov, A.; Schmidt, L.; Tsipras, D.; and Vladu, A. 2017. Towards deep learning models resistant to adversarial attacks. *arXiv preprint arXiv:1706.06083*.
- Mannos, J.; and Sakrison, D. 1974. The effects of a visual fidelity criterion of the encoding of images. *IEEE transactions on Information Theory*, 20(4): 525–536.
- Mitsa, T.; and Varkur, K. L. 1993. Evaluation of contrast sensitivity functions for the formulation of quality measures incorporated in halftoning algorithms. In *1993 IEEE International Conference on Acoustics, Speech, and Signal Processing*, volume 5, 301–304. IEEE.
- Mittal, A.; Moorthy, A. K.; and Bovik, A. C. 2011. Blind/referenceless image spatial quality evaluator. In *2011 conference record of the forty fifth asilomar conference on signals, systems and computers (ASILOMAR)*, 723–727. IEEE.
- Mittal, A.; Soundararajan, R.; and Bovik, A. C. 2012. Making a “completely blind” image quality analyzer. *IEEE Signal processing letters*, 20(3): 209–212.
- Modas, A.; Moosavi-Dezfooli, S.-M.; and Frossard, P. 2019. Sparsefool: a few pixels make a big difference. In *Proceedings of the IEEE/CVF conference on computer vision and pattern recognition*, 9087–9096.
- Mou, C.; Wang, X.; Xie, L.; Zhang, J.; Qi, Z.; Shan, Y.; and Qie, X. 2023. T2i-adapter: Learning adapters to dig out more controllable ability for text-to-image diffusion models. *arXiv preprint arXiv:2302.08453*.
- Nichol, A.; Dhariwal, P.; Ramesh, A.; Shyam, P.; Mishkin, P.; McGrew, B.; Sutskever, I.; and Chen, M. 2021. Glide: Towards photorealistic image generation and editing with text-guided diffusion models. *arXiv preprint arXiv:2112.10741*.
- Podell, D.; English, Z.; Lacey, K.; Blattmann, A.; Dockhorn, T.; Müller, J.; Penna, J.; and Rombach, R. 2023. Sdxl: improving latent diffusion models for high-resolution image synthesis. *arXiv preprint arXiv:2307.01952*.
- Prashnani, E.; Cai, H.; Mostofi, Y.; and Sen, P. 2018. Pieapp: Perceptual image-error assessment through pairwise preference. In *Proceedings of the IEEE Conference on Computer Vision and Pattern Recognition*, 1808–1817.
- Radford, A.; Kim, J. W.; Hallacy, C.; Ramesh, A.; Goh, G.; Agarwal, S.; Sastry, G.; Askell, A.; Mishkin, P.; Clark, J.; et al. 2021. Learning transferable visual models from natural language supervision. In *International conference on machine learning*, 8748–8763. PMLR.
- Rombach, R.; Blattmann, A.; Lorenz, D.; Esser, P.; and Ommer, B. 2022. High-resolution image synthesis with latent diffusion models. In *Proceedings of the IEEE/CVF conference on computer vision and pattern recognition*, 10684–10695.
- Ruiz, N.; Bargal, S. A.; and Sclaroff, S. 2020a. Disrupting deepfakes: Adversarial attacks against conditional image translation networks and facial manipulation systems. In *Computer Vision—ECCV 2020 Workshops: Glasgow, UK, August 23–28, 2020, Proceedings, Part IV 16*, 236–251. Springer.
- Ruiz, N.; Bargal, S. A.; and Sclaroff, S. 2020b. Protecting against image translation deepfakes by leaking universal perturbations from black-box neural networks. *arXiv preprint arXiv:2006.06493*.
- Ruiz, N.; Li, Y.; Jampani, V.; Pritch, Y.; Rubinstein, M.; and Aberman, K. 2023. Dreambooth: Fine tuning text-to-image diffusion models for subject-driven generation. In *Proceedings of the IEEE/CVF Conference on Computer Vision and Pattern Recognition*, 22500–22510.
- Saharia, C.; Chan, W.; Saxena, S.; Li, L.; Whang, J.; Denton, E. L.; Ghasemipour, K.; Gontijo Lopes, R.; Karagol Ayan, B.; Salimans, T.; et al. 2022. Photorealistic text-to-image diffusion models with deep language understanding. *Advances in Neural Information Processing Systems*, 35: 36479–36494.
- Salman, H.; Khaddaj, A.; Leclerc, G.; Ilyas, A.; and Madry, A. 2023. Raising the cost of malicious ai-powered image editing. *arXiv preprint arXiv:2302.06588*.
- Schölkopf, B.; Smola, A. J.; Williamson, R. C.; and Bartlett, P. L. 2000. New support vector algorithms. *Neural computation*, 12(5): 1207–1245.
- Sen, A.; Zhu, X.; Marshall, L.; and Nowak, R. 2019. Should adversarial attacks use pixel p-norm? *arXiv preprint arXiv:1906.02439*.
- Shamsabadi, A. S.; Sanchez-Matilla, R.; and Cavallaro, A. 2020. Colorfool: Semantic adversarial colorization. In *Proceedings of the IEEE/CVF conference on computer vision and pattern recognition*, 1151–1160.
- Shan, S.; Cryan, J.; Wenger, E.; Zheng, H.; Hanocka, R.; and Zhao, B. Y. 2023. Glaze: Protecting artists from style mimicry by text-to-image models. *arXiv preprint arXiv:2302.04222*.
- Shen, Z.; Fan, S.; Wong, Y.; Ng, T.-T.; and Kankanhalli, M. 2019. Human-imperceptible privacy protection against machines. In *Proceedings of the 27th ACM international conference on multimedia*, 1119–1128.
- Sohn, K.; Ruiz, N.; Lee, K.; Chin, D. C.; Blok, I.; Chang, H.; Barber, J.; Jiang, L.; Entis, G.; Li, Y.; et al. 2023. StyleDrop: Text-to-Image Generation in Any Style. *arXiv preprint arXiv:2306.00983*.
- Tan, W. R.; Chan, C. S.; Aguirre, H. E.; and Tanaka, K. 2018. Improved ArtGAN for conditional synthesis of natural image and artwork. *IEEE Transactions on Image Processing*, 28(1): 394–409.
- Van Le, T.; Phung, H.; Nguyen, T. H.; Dao, Q.; Tran, N. N.; and Tran, A. 2023. Anti-DreamBooth: Protecting users from personalized text-to-image synthesis. In *Proceedings of the IEEE/CVF International Conference on Computer Vision*, 2116–2127.
- Wang, Y.; Wu, S.; Jiang, W.; Hao, S.; Tan, Y.-a.; and Zhang, Q. 2021. Demiguise attack: Crafting invisible semantic adversarial perturbations with perceptual similarity. *arXiv preprint arXiv:2107.01396*.

Wang, Z.; Bovik, A. C.; Sheikh, H. R.; and Simoncelli, E. P. 2004. Image quality assessment: from error visibility to structural similarity. *IEEE transactions on image processing*, 13(4): 600–612.

Wei, Z.; and Ngan, K. N. 2009. Spatio-temporal just noticeable distortion profile for grey scale image/video in DCT domain. *IEEE Transactions on Circuits and Systems for Video Technology*, 19(3): 337–346.

Wu, J.; Lin, W.; Shi, G.; Wang, X.; and Li, F. 2013a. Pattern masking estimation in image with structural uncertainty. *IEEE Transactions on Image Processing*, 22(12): 4892–4904.

Wu, J.; Shi, G.; and Lin, W. 2019. Survey of visual just noticeable difference estimation. *Frontiers of Computer Science*, 13: 4–15.

Wu, J.; Shi, G.; Lin, W.; Liu, A.; and Qi, F. 2013b. Just noticeable difference estimation for images with free-energy principle. *IEEE Transactions on Multimedia*, 15(7): 1705–1710.

Xiang, C. 2022. Artists Are Revolting Against AI Art on ArtStation. *Vice*.

Ye, X.; Huang, H.; An, J.; and Wang, Y. 2023. DUAW: Data-free Universal Adversarial Watermark against Stable Diffusion Customization. *arXiv preprint arXiv:2308.09889*.

Zhang, L.; Rao, A.; and Agrawala, M. 2023. Adding conditional control to text-to-image diffusion models. In *Proceedings of the IEEE/CVF International Conference on Computer Vision*, 3836–3847.

Zhang, R.; Isola, P.; Efros, A. A.; Shechtman, E.; and Wang, O. 2018. The unreasonable effectiveness of deep features as a perceptual metric. In *Proceedings of the IEEE conference on computer vision and pattern recognition*, 586–595.

Zhao, Z.; Duan, J.; Hu, X.; Xu, K.; Wang, C.; Zhang, R.; Du, Z.; Guo, Q.; and Chen, Y. 2023. Unlearnable Examples for Diffusion Models: Protect Data from Unauthorized Exploitation. *arXiv preprint arXiv:2306.01902*.

Zhao, Z.; Liu, Z.; and Larson, M. 2020. Towards large yet imperceptible adversarial image perturbations with perceptual color distance. In *Proceedings of the IEEE/CVF Conference on Computer Vision and Pattern Recognition*, 1039–1048.

Zheng, B.; Liang, C.; Wu, X.; and Liu, Y. 2023. Understanding and Improving Adversarial Attacks on Latent Diffusion Model. *arXiv preprint arXiv:2310.04687*.

Appendix

Related Work

Image protection against generative models. The adversarial examples have also been applied to generative models to prevent the misuse of deepfake technology. For example, Ruiz, Bargal, and Sclaroff (2020a) introduced adversarial attacks against deepfake image translation systems, proposing methods such as class-transferable attacks and adversarial training to disrupt manipulated images and evade defenses. Similarly, Ruiz, Bargal, and Sclaroff (2020b) proposed a novel perturbation algorithm that effectively disrupts black-box image translation models.

More recently, the diffusion models have significantly improved their ability to generate images with high fidelity. While these developments provide substantial benefits, they have also led to more severe misuse. Consequently, recent studies on image protection have increasingly focused on the diffusion models. Most of them have explored the iterative optimization of adversarial perturbations by adapting the loss functions of diffusion models. For example, nearly all diffusion-based protection frameworks update perturbations using either the loss in Eq. 2 or Eq. 3. The former approach employs the encoder or texture loss, as seen in methods like PhotoGuard (Salman et al. 2023) and GLAZE (Shan et al. 2023). The latter adopts the diffusion or semantic loss, exemplified by frameworks such as AdvDM (Liang et al. 2023) and Anti-DreamBooth (Van Le et al. 2023). Furthermore, some approaches combine these losses (Liang and Wu 2023), while others incorporate additional losses (Shan et al. 2023; Ye et al. 2023) or logic (Van Le et al. 2023) to develop more effective protection methods.

Imperceptible adversarial examples. The concept of imperceptibility has been actively investigated in adversarial attacks (Luo et al. 2018; Guo, Frank, and Weinberger 2018; Shen et al. 2019; Sen et al. 2019; Modas, Moosavi-Dezfooli, and Frossard 2019; Croce and Hein 2019; Shamsabadi, Sanchez-Matilla, and Cavallaro 2020; Zhao, Liu, and Larson 2020; Wang et al. 2021; Luo et al. 2022; Dai et al. 2023). Among them, some studies target specific elements; e.g. the low-frequency components (Guo, Frank, and Weinberger 2018; Luo et al. 2022). Another approach use advanced constraints (Sen et al. 2019); color distance (Zhao, Liu, and Larson 2020) or quality assessment (Wang et al. 2021) are adopted. Several methods focus on restricting perturbation regions; leveraging L_0 norm to produce sparse perturbation (Modas, Moosavi-Dezfooli, and Frossard 2019; Croce and Hein 2019) or limiting perturbations to tiny salient regions (Dai et al. 2023). Our research draws inspiration from these studies. However, attacking discriminative models is fundamentally distinct from that of targeting generative models. Hence, we employ a specialized strategy designed specifically for disrupting style imitation.

Method Details

In this section, we describe the details of IMPASTO— the computation and discussion of JND estimations, perceptual constraints, and the implementation specifics.

JND Estimations

In our study, we investigated five widely-used JND models, briefly illustrated below.

- **Luminance adaptation (LA):** Perturbations are less visible in regions of very low or high luminance and more noticeable in moderate lighting conditions (Jarsky et al. 2011). Hence, we modulate protection strength based on pixel luminance with a fixed adaptation model.
- **Contrast masking (CM):** Perturbations can seamlessly blend into regions with intricate textures, while they leave distinct traces on flat surfaces. To simulate this, we utilize the luminance contrast (or change) of a region to measure the complexity of the pixel (Legge and Foley 1980; Wu et al. 2013a).
- **Contrast sensitivity function (CSF):** Given the band-pass characteristics of the human visual system, we utilize a frequency-based JND model (Wei and Ngan 2009). The human eye is receptive to signals at modulated frequencies while exhibiting insensitivity to high-frequency components. Consequently, perturbations overlaid on high-frequency signals (e.g. edges) are less perceptible.
- **Standard deviation:** To assess the spatial structure of an image, we calculate the standard deviation of local image blocks, inspired by SSIM (Wang et al. 2004). This measures the image’s structural complexity, which correlates with the sensitivity to subtle perturbations.
- **Entropy:** The entropy of an image block is computed to quantify the amount of information or complexity within a local region (Wu et al. 2013b).

We also provide a more comprehensive elucidation of the fundamental rationale of these estimations and delve into the specifics of their computations:

Luminance adaptation. The visibility thresholds within the human visual system vary to luminance levels (Jarsky et al. 2011). For instance, our eye is more sensitive under moderate lighting conditions, while discrimination is challenging in a very dark light. Similarly, we observed that perturbations are less noticeable in regions with extremely low or high luminance, prompting an increase in protection strength within these areas. To implement this concept, luminance adaptation is computed following Chou and Li (Chou and Li 1995) as in the below equation.

$$LA(\mathbf{x}) = \begin{cases} 17 \times (1 - \sqrt{\frac{B(\mathbf{x})}{127}}) + 3, & \text{if } B(\mathbf{x}) \leq 127 \\ \frac{3}{128} \times (B(\mathbf{x}) - 127) + 3, & \text{otherwise,} \end{cases} \quad (14)$$

where $B(\mathbf{x})$ is the background luminance, which is calculated as the mean luminance of a local 3×3 block. With this formulation, the sensitivity (the inverse of LA) peaks at luminance ranging from 100 to 200. As luminance approaches an extremely low value (darker area), human perception fails to discern minor variations. Conversely, at high luminance levels, the detection ability becomes progressively more difficult, albeit less so compared to the darker regions.

Contrast masking. It is obvious that stimuli become less perceptible against patterned, non-uniform backgrounds. In our context, perturbations can seamlessly blend into regions with intricate textures, while they leave distinct traces on flat surfaces. To simulate this effect, we first compute the luminance contrast (Legge and Foley 1980) by convolving an input image with four directional filters. This process highlights the complexity of a region by contrasting it with its immediate surroundings. Subsequently, contrast masking is established by mapping the luminance contrast onto a logarithmic curve (Wu et al. 2013a).

$$CM(\mathbf{x}) = 0.115 \times \frac{16 \times LC(\mathbf{x})^{2.4}}{LC(\mathbf{x})^2 + 26^2}, \quad (15)$$

where luminance contrast $LC(\mathbf{x})$ is obtained via four directional filters as $LC(\mathbf{x}) = \frac{1}{16} \times \max_{k=1,\dots,4} |\mathbf{x} * \nabla_k|$ following Wu et al. (Wu, Shi, and Lin 2019).

Contrast sensitivity function. The human visual system exhibits a band-pass response to spatial frequency and CSF represents a function of how our eye is sensitive to the contrast of signals at various spatial frequencies. High spatial frequencies correspond to rapid changes in image details, and contrast sensitivity is optimal at moderate spatial frequencies. Beyond a certain frequency threshold, known as the resolution limit, our eyes are unable to detect changes. Upon this concept, several studies have introduced and modified the CSF (Larson and Chandler 2010; Mitsa and Varkur 1993; Damera-Venkata et al. 2000; Mannos and Sakrison 1974); the CSF model $H(f, \theta)$ is given below.

$$H = \begin{cases} 2.6 \times (\alpha + \beta f_\theta) e^{-(\beta f_\theta)^{1.1}}, & \text{if } f \geq 7.8909 \\ 0.981, & \text{otherwise,} \end{cases} \quad (16)$$

where $\alpha = 0.0192$, $\beta = 0.114$ and f is the radial spatial frequency, measured in cycles per degree of visual angle (c/deg). The variable θ , ranging from $[-\pi, \pi]$, denotes the orientation. Additionally, $f_\theta = f / [0.15 \times \cos(4\theta) + 0.85]$ accounts for the oblique effect (Larson and Chandler 2010). The CSF model is now applied to an image in the frequency domain as $\mathbf{x}_{csf} = \mathcal{F}^{-1}[H(u, v) \times \mathcal{F}(\tilde{\mathbf{x}})]$, where $\mathcal{F}[\cdot]$ and $\mathcal{F}^{-1}[\cdot]$ represent the DFT and its inverse, respectively. Here, $H(u, v)$ is the DFT-version of $H(f, \theta)$, with u, v being the DFT indices. The transformation from $H(f, \theta)$ to $H(u, v)$ is elaborated in Larson et al. (Larson and Chandler 2010). Prior to applying the CSF model, an input image \mathbf{x} is converted into a perception-adjusted luminance form to reflect the non-linear relationship between digital pixel values and physical luminance (Larson and Chandler 2010). This is achieved by calibrating \mathbf{x} to the settings of an sRGB display and converting it into perceived luminances, which indicates the relative lightness: $\tilde{\mathbf{x}} = \sqrt[3]{(0.02874\mathbf{x})^{2.2}}$.

Standard deviation. It has served as a crucial metric for quantifying the structural information of an image, both in pixel space (Wang et al. 2004) and feature space (Ding et al. 2020). Given that perturbations tend to be less noticeable in areas exhibiting high levels of change, (as discussed in contrast masking), we focus on these sudden changes, interpreting them as structural components. For this purpose,

we compute the block-wise standard deviation in pixel space using a 9×9 local block.

Entropy. Similar to standard deviation, block-wise entropy is calculated using a 9×9 local window. This approach is based on the concept that the complexity of a local region influences the detectability of subtle perturbations. The higher the local entropy, the more intricate the region, potentially rendering minor perturbations less perceptible.

Post-processing All the JND estimations are min-max normalized and then inverted by subtracting from one. When constructing a perceptual map \mathcal{M} with JND estimations, we encountered issues with some JNDs displaying extremely skewed distributions. Additionally, the distributions of JNDs often do not align with each other, posing challenges in their combination. While standardization aligns the distributions, we found that the continuous JND values provide weak signals as masks (e.g. on average, the protection strength drops to 50% compared to the original). To give a more distinct signal depending on the JND values, we discretize the scores by quantizing the JND values. This involves calculating JND quantiles, where the first quantile is set to 1.0. For each subsequent quantile, we multiply by a factor of β to decrease the value in a discrete manner. We use $\beta = 0.85$, resulting in quantized JND values across four quantiles as [1.0, 0.85, 0.7225, 0.6141]. This allows for a more nuanced adjustment of the protection intensity while accommodating the varied distributions of JND estimations.

Perceptual Constraints

Masked LPIPS. We use AlexNet (Krizhevsky, Sutskever, and Hinton 2012) as the backbone network for the LPIPS loss, adhering to the parameter settings in the official LPIPS implementation.

Masked low-pass. In this constraint, we utilize $LP(\cdot)$, a reconstruction function focusing on the low-frequency component. Inspired by Luo et al. (Luo et al. 2022), we implement a DWT-based reconstruction module. Given an input image \mathbf{x} , DWT decomposes it into one low-frequency component and three high-frequency components, as expressed by the following equation.

$$\begin{aligned} \mathbf{x}_{ll} &= \mathbf{L}\mathbf{x}\mathbf{L}^T, & \mathbf{x}_{lh} &= \mathbf{H}\mathbf{x}\mathbf{L}^T, \\ \mathbf{x}_{hl} &= \mathbf{L}\mathbf{x}\mathbf{H}^T, & \mathbf{x}_{hh} &= \mathbf{H}\mathbf{x}\mathbf{H}^T. \end{aligned} \quad (17)$$

\mathbf{L} and \mathbf{H} represent the low-pass and high-pass filters of an orthogonal wavelet, respectively. To reconstruct an image using only its low-frequency component, we input \mathbf{x}_{ll} alone into the inverse DWT function. Thus, $LP(\mathbf{x})$ is defined as:

$$LP(\mathbf{x}) = \mathbf{L}^T \mathbf{x}_{ll} \mathbf{L} = \mathbf{L}^T (\mathbf{L}\mathbf{x}\mathbf{L}^T) \mathbf{L}. \quad (18)$$

CLIP. As outlined in Eq. 12, IMPASTO focuses on maximizing the feature distance between the protected image and the prompt $C = \text{“Noise-free image”}$. While it is conceivable to minimize the distance using a ‘bad’ prompt (e.g. $C = \text{“noisy image”}$) or to integrate both ‘good’ and ‘bad’ prompts, we observed that all these show comparable performance. Therefore, we opted to employ the ‘good’ prompt only in the CLIP-based constraint.

Table 4: **Component analysis.** Within IMPASTO, we conduct an analysis by excluding the JND-based perceptual map generation, resulting in the creation of the perceptual map from random masks (denoted as w/o JND). Additionally, we evaluate the impact of omitting the perception-aware protection (denoted as w/o PAP).

Method	Protected Image Quality		Protection Performance	
	DISTS (\downarrow)	TOPIQ (\uparrow)	BRISQUE (\uparrow)	FID (\uparrow)
IMPASTO (Full model)	0.159	0.912	20.74	279.3
w/o JND	0.158	0.912	19.30	268.1
w/o PAP	0.199	0.890	17.57	281.1

Table 5: **Evaluating the impact of varying refinement interval step P .** In this analysis, we assess the impact on performance by varying the refinement interval step P for executing IWR and DAP.

Method	Protected Image Quality		Protection Performance	
	DISTS (\downarrow)	TOPIQ (\uparrow)	BRISQUE (\uparrow)	FID (\uparrow)
$P = 1$	0.159	0.913	19.29	278.4
$P = 2$	0.158	0.913	18.19	279.7
$P = 4$	0.159	0.912	20.74	279.3
$P = 10$	0.159	0.913	18.49	274.3

Implementation Details

When we implement IMPASTO into the existing protection methods, we adhere to their respective settings. Regarding the IMPASTO’s own components, we use following hyperparameters depicted in Eq. 13 as: $\lambda_L = 5.0, \lambda_{LP} = 10.0, \lambda_C = 0.1$. For our PAP (Eq. 6), we utilize the L_∞ norm. On the other hand, for the IWR loss (Eq. 7), we employ the L_2 norm. When we calculate IWR loss, since the distance between \mathcal{L}_{SP} respect to \mathcal{M}' and $\mathcal{M}(\omega)$ (first term) is significantly smaller than the L_2 constraint (second term), we amplify the former term by a factor of 5×10^7 . For difficulty prediction in DAP, we set $t = 5$ with $T = 25$. We execute IWR and DAP every $P = 4$ steps. On an NVIDIA A100 GPU, the overall perturbation optimization takes about 30 seconds for a single 512×512 resolution image.

In addition, during our experiments, we observed that the magnitudes of \mathcal{L}_E and \mathcal{L}_{SD} differ considerably, with the SD loss exhibiting much smaller values. Hence, when integrating IMPASTO into UNet-based protection methods (e.g. AdvDM (Liang et al. 2023), Anti-DreamBooth (Van Le et al. 2023), Mist (Liang and Wu 2023)), we scale down $\lambda_L, \lambda_{LP}, \lambda_C$ by a factor of 0.05. This adjustment is made to balance the influence of our proposed components, ensuring that the impact of IMPASTO is consistent and effective in enhancing image protection.

Experimental Settings

Datasets. In our study, we chose the painting and cartoon domains, which are most significantly impacted by style imitation from diffusion models, and used them as benchmark datasets. To create the “painting” dataset, we gather artworks from the WikiArt dataset (Tan et al. 2018). This dataset includes selections from 15 artists, 10 artworks per each. The “cartoon” dataset is sourced from the NAVER WEBTOON platform; images are cropped to contain only character depictions. This comprises 15 cartoons with 10 cartoon character images each. Following previous dataset preparation protocols (Van Le et al. 2023), each image was resized to

512×512 . And note that as IMPASTO does not require a separate training process, the data was used as benchmark set.

Evaluation. To assess the quality of the protected images, we utilize three deep learning-based full-reference quality assessments: DISTS (Ding et al. 2020), PieAPP (Prashnani et al. 2018), and TOPIQ (Chen et al. 2023). These measures compare the protected images against the original artworks. DISTS is designed to be sensitive to structural changes while exhibiting explicit tolerance to texture resampling. It achieves this by evaluating both the mean and correlation of feature maps from the compared images. PieAPP measures the perceptual error of a distorted image with respect to a reference and its training dataset. TOPIQ adopts a top-down approach, leveraging high-level semantics to direct the quality assessment network’s focus towards semantically significant local distortion regions.

To evaluate protection performance, we employ NIQE (Mittal, Soundararajan, and Bovik 2012), BRISQUE (Mittal, Moorthy, and Bovik 2011), and FID (Heusel et al. 2017). NIQE and BRISQUE are blind image quality assessment methods that only use generated images for evaluation. BRISQUE operates on the premise that distortions in natural images disrupt pixel distributions. It processes an input image and then extracts features, which are finally mapped to a mean opinion score with SVM regressor (Schölkopf et al. 2000). NIQE, in contrast, does not rely on opinion scores, instead assesses the quality of an image by comparing its statistical properties with those of a clean image dataset.

It is important to note that some protection assessments, such as NIQE and BRISQUE, despite their widespread use, have limitations in our context: 1) They are designed primarily for natural image domains, making their measurements potentially unreliable in artistic domains, particularly for cartoons. 2) Traditional non-reference assessments focus on common distortions such as JPEG compression, blurring, and Gaussian noise, which may not effectively capture the unique artifacts in generated images in our task. Therefore, these metrics tend to fluctuate instead of showing a consis-

Table 6: **Quantitative comparison** of protection methods with and without IMPASTO. Unlike Table 1, we match the protected image quality to a similar level and compare the protection performance.

Dataset	Method	Protected Image Quality			Protection Performance		
		DISTS (\downarrow)	PieAPP (\downarrow)	TOPIQ (\uparrow)	NIQE (\uparrow)	BRISQUE (\uparrow)	FID (\uparrow)
Painting	PhotoGuard	0.181	0.364	0.896	4.306 (+0.000)	20.99 (+0.00)	277.6 (+0.0)
	+ IMPASTO	0.186	0.346	0.889	4.451 (+0.145)	22.02 (+1.03)	286.9 (+9.3)
	AdvDM	0.167	0.730	0.846	3.761 (+0.000)	12.45 (+0.00)	269.0 (+0.0)
	+ IMPASTO	0.164	0.503	0.842	3.947 (+0.231)	11.60 (-0.85)	276.6 (+7.6)
Cartoon	PhotoGuard	0.249	0.782	0.797	5.037 (+0.000)	10.19 (+0.00)	155.9 (+0.0)
	+ IMPASTO	0.241	0.894	0.779	5.480 (+0.443)	12.88 (+2.69)	162.5 (+6.6)
	AdvDM	0.241	0.776	0.775	4.802 (+0.000)	10.95 (+0.00)	153.5 (+0.0)
	+ IMPASTO	0.243	0.819	0.744	4.780 (-0.022)	11.90 (+0.95)	155.9 (+2.4)

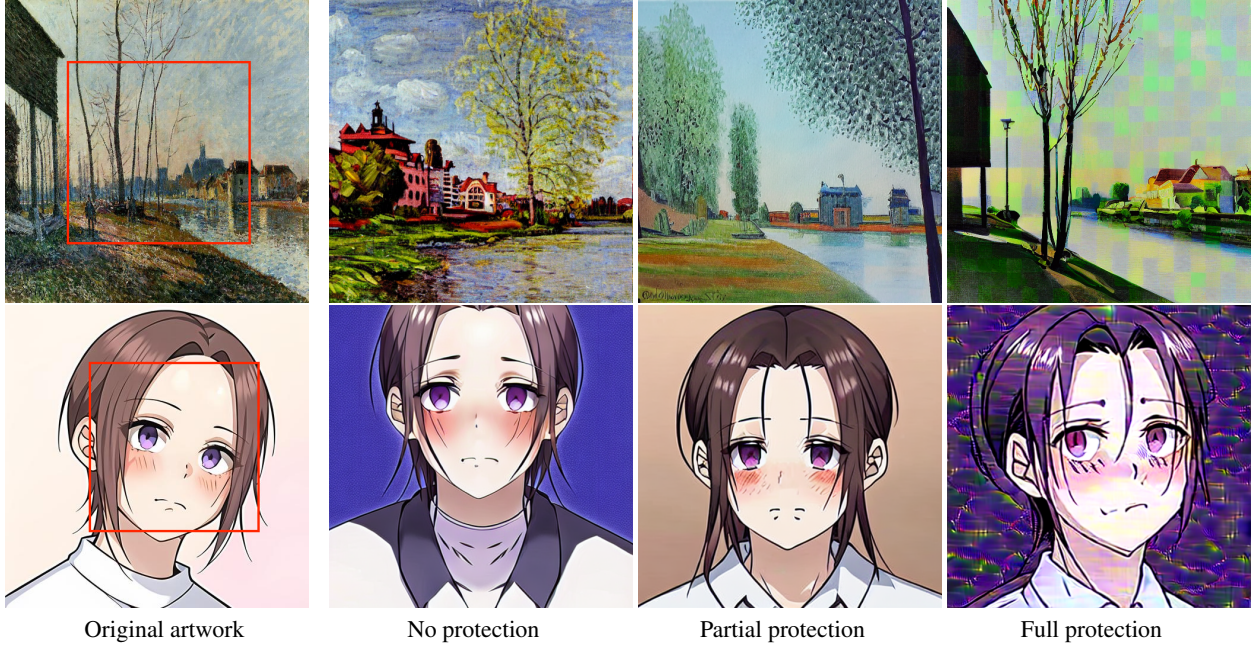


Figure 11: **Comparison of restriction types.** Extending Figure 2, we compare the fine-tuning results of the original artwork with no protection, partial protection, and full protection. The red inset in the original artwork highlights the area where perturbations were applied in the partial protection case, with perturbations confined to the inset.

tent progression with varying protection strengths. FID, although potentially inconsistent due to a limited number of evaluation samples, aligns more closely with human preferences in this task. We suspect that it because FID measures the distance between two distributions—the original artwork and the generated image—providing more reliable assessments. Therefore, we further validated IMPASTO’s effectiveness through human evaluation.

User study. We conducted a user study in the form of an A/B test with a reference image as a benchmark. A total of 44 participants were involved, tasked with determining the better-quality protected image (given the reference original artwork) and identifying the lower-quality generated image (given a reference DreamBooth (Ruiz et al. 2023) generated image). Each participant was asked to vote on 8 questions for PhotoGuard (Salman et al. 2023) and another 9 for AdvDM (Liang et al. 2023).

Discussions and Analyses

Full vs. partial protection. Extending Figure 2, in Figure 11, we compare the original artwork, and the personalization results of unprotected, partially protected, and fully protected artworks. Partial protection simulates hard restrictions, whereas full protection mimics soft restrictions. To create partially protected images, we apply protection to the center (Figure 11, top) or the facial region (Figure 11, bottom), as indicated by the red boxes. Both the unprotected and partially protected images cannot prevent against style imitation from the personalization method. In contrast, full protection (soft restriction) successfully prevents this.

We also conduct a quantitative comparison between partial and full protection with FID on the painting dataset. In this experiment, the partial protection achieves 260.2, while full protection scores 299.1, demonstrating the higher efficacy of full protection. This empirical evidence led us to

Table 7: **Quantitative comparison** on facial datasets.

Dataset	Method	Protected Image Quality			Protection Performance		
		DISTS (\downarrow)	PicAPP (\downarrow)	TOPIQ (\uparrow)	NIQE (\uparrow)	BRISQUE (\uparrow)	FID (\uparrow)
CelebA-HQ	PhotoGuard	0.280 (+0.000)	0.379 (+0.000)	0.878 (+0.000)	5.031	15.36	233.1
	+ IMPASTO	0.266 (+0.014)	0.376 (+0.003)	0.880 (+0.002)	5.161	14.13	234.6
	AdvDM	0.213 (+0.000)	0.573 (+0.000)	0.832(+0.000)	4.051	10.05	278.8
	+ IMPASTO	0.195 (+0.018)	0.522 (+0.051)	0.854(+0.022)	4.080	10.59	273.6
VGGFace2	PhotoGuard	0.270 (+0.000)	0.413 (+0.000)	0.870 (+0.000)	5.916	19.73	253.9
	+ IMPASTO	0.255 (+0.015)	0.413 (+0.000)	0.868 (-0.002)	5.746	19.39	257.0
	AdvDM	0.206 (+0.000)	0.589 (+0.000)	0.821 (+0.000)	3.977	8.43	292.9
	+ IMPASTO	0.187 (+0.019)	0.543 (+0.043)	0.846 (+0.025)	3.986	9.86	289.8

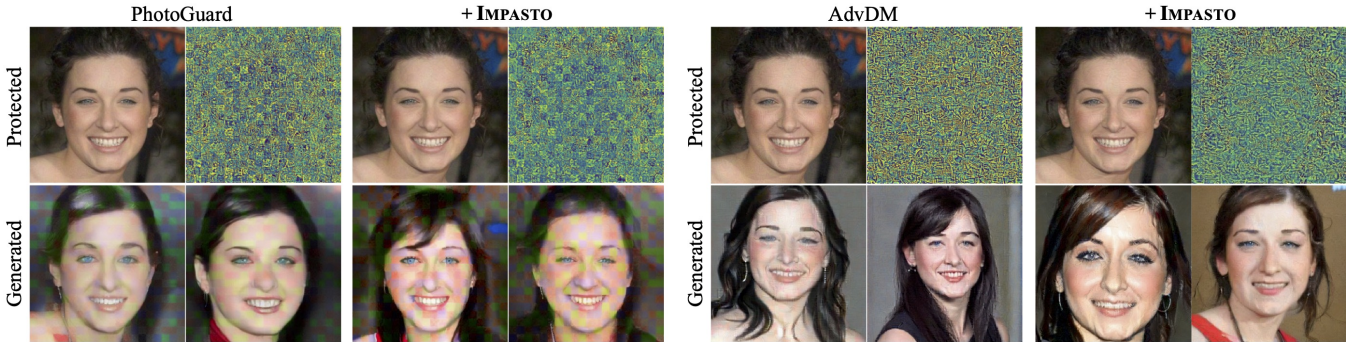


Figure 12: **Qualitative comparison** on facial dataset.

propose soft restriction-based JND perceptual protection.

JNDs. In this section, we further analyze the protection performance of JND-based perception map depicted in Figure 3 (right). When compared to the baseline, perceptual map improves image quality (DISTS) across the board, but it also leads to a compromise in protection performance (FID). Among the JNDs, LA demonstrates the best protection performance. We conjecture that in many artworks, the majority of areas fall high or low-luminance, thereby maintaining perturbations strength high across extensive regions. However, as shown in upper image, even simple textures (*e.g.* sky) can have strong perturbations, placing LA at the lower image quality. On the other hand, CSF, Std, and Entropy generally apply high perturbations only to specific areas, such as edges, resulting in most regions being not fully protected and consequently, causing a huge degradation in protection performance. CM’s protection intensity is also determined by spatial changes but this covers more detailed local regions (see *fields* in upper image) and also being based on contrast, leading to both high quality and effective protection.

Ablation study. In Table 2, one might expect that the JND (PAP with JND) maintains protection scores while improving image quality. Indeed, the random mask (PAP without JND) constrains the protection intensity in a similar level to the JND-based map. This is because both maps are normalized between 0 and 1. As a result, they yield similar perturbation magnitudes, leading to a comparable image quality. Nonetheless, the JND-based perceptual map prioritizes less sensitive regions for perturbation while reducing it in highly sensitive areas. Despite the similar protection magnitudes, the JND-based PAP achieves more effective protection. This

hints at the possibility that the JND maps are helpful in finding the areas that are important for style protection. For instance, in areas with complex textures, the PAP applies more perturbations than its non-JND counterpart. However, these perturbations are typically imperceptible to humans, thereby ensuring perceptually acceptable image quality.

In Table 4, we show additional analysis by omitting certain components from the full IMPASTO framework. Specifically, we assess the impact of 1) removing the JND-based perception map, which results in initializing M with random masks (w/o JND), and 2) excluding the proposed perception-aware protection (PAP), thereby relying solely on the perceptual constraint bank (w/o PAP). For the w/o JND case, in contrast to Table 2, we start with a full-component model and remove only the JND part. The results indicate that discarding the JNDs leads to a decrease in protection performance while maintaining similar image quality, corroborating the findings in Table 2. When PAP is not applied, there is a slight increase in protection performance (FID: 279.3 \rightarrow 281.1) with significant compromise on image quality. These observations suggest that the integration of PAP alongside a JND-based perceptual map is crucial for achieving an imperceptible style protection framework that effectively balances protection performance with image quality.

Varying refinement interval step. In this analysis, we explore the effect of varying the refinement interval step P on instance-wise refinement (IWR) and difficulty-aware protection (DAP) to evaluate changes in protection performance (Table 5). We observe that even as P increases from 1 to 4 (*i.e.*, with less frequent refinements), both image quality and protection capability remain relatively stable. This stability

Table 8: **Quantitative comparison** of protection methods w/ and w/o IMPASTO, both selected for their comparable protection performance. IMPASTO markedly elevates the protected images’ quality while maintaining protection efficacy.

Dataset	Method	Protected Image Quality			Protection Performance		
		DISTS (\downarrow)	LPIPS (\downarrow)	TOPIQ (\uparrow)	NIQE (\uparrow)	BRISQUE (\uparrow)	FID (\uparrow)
Painting	Anti-DB	0.151 (+0.000)	0.081 (+0.000)	0.876 (+0.000)	3.865	13.63	266.1
	+ IMPASTO	0.138 (+0.013)	0.008 (+0.073)	0.889 (+0.013)	3.780	12.60	270.9
	Mist	0.167 (+0.000)	0.100 (+0.000)	0.846(+0.000)	4.052	13.96	272.2
	+ IMPASTO	0.144 (+0.023)	0.077 (+0.023)	0.879(+0.033)	3.830	11.11	273.0
Cartoon	Anti-DB	0.260 (+0.000)	0.154 (+0.000)	0.700(+0.000)	4.437	15.48	160.6
	+ IMPASTO	0.234 (+0.026)	0.027 (+0.127)	0.782(+0.092)	4.589	12.35	161.0
	Mist	0.256 (+0.000)	0.160 (+0.000)	0.709(+0.000)	4.597	10.86	158.7
	+ IMPASTO	0.238 (+0.018)	0.077 (+0.083)	0.772(+0.063)	4.693	11.23	158.3

can be attributed to the initial use of a JND-based perceptual map \mathcal{M} , which requires only minor adjustments during the IWR step. However, when P is increased to 10, a significant reduction in protection performance is observed, indicating that such a large interval is insufficient for optimal refinement. Therefore, we set $P = 4$ as the default, balancing performance efficacy with the number of optimization steps.

Table 9: **Comparison on the blur countermeasure** of PhotoGuard with and without IMPASTO at a similar level of protected image quality.

FID (\uparrow)	PhotoGuard	+ IMPASTO
Clean	274.4	279.3
Blur	273.5	274.6

Countermeasures. As discussed earlier, IMPASTO achieves similar protection performance against JPEG compression and Gaussian noise countermeasures but shows slight degradation under Gaussian blur. The reason for this phenomenon is that the blurring effect removes most high-frequencies, making weak perturbations less effective. We note that if baseline protection models are applied with weak protection strength (to match the protected images’ perceptual quality to ours), they also exhibit degraded protection performance.

To demonstrate this, we match the protected image quality of PhotoGuard to ours and compare the protection performance in both clean (no countermeasure) and blur scenarios (Table 9). In this case, which with similar imperceptibility, IMPASTO shows better performance under blur, implying that such degradation is an inevitable limitation of using weaker perturbations rather than a flaw in our model design. Note that the performance gap narrows under blur because IMPASTO applies very weak perturbations to more noticeable regions, potentially causing minor vulnerabilities. Nevertheless, in all scenarios—whether clean or under countermeasures—IMPASTO demonstrates an improved trade-off between protected image quality and protection performance, highlighting its practical effectiveness.

Protection performance comparison. Here, unlike Table 1, which compares the protected images’ quality under similar protection performance, we compare the protection performance while fixing the image quality. In Table 6, IMPASTO improves protection performance compared to the baseline

in most metrics and scenarios. This was also shown in the quality-protection trade-off (Figure 7). These results indicate that attaching IMPASTO to the protection baselines enables them to be better protection methods.

IMPASTO in other domain. Although IMPASTO is initially proposed to prevent style imitation, its applicability can be extended beyond other domains or applications. To validate this, we conduct protection on two facial datasets, CelebA-HQ (Karras et al. 2017) and VGGFace2 (Cao et al. 2018). As demonstrated in Table 7 and Figure 12, adopting IMPASTO in these natural domains can also enhance the quality of protected images without compromising the protection performance of baseline models. This broad applicability highlights IMPASTO’s versatility and potential as a universal tool for protecting users’ copyright and preventing serious threats of deepfakes.

Additional Results

IMPASTO with other protection methods. In addition to PhotoGuard (Salman et al. 2023) and AdvDM (Liang et al. 2023), we extend the application of IMPASTO to recent protection techniques, Anti-DreamBooth (Van Le et al. 2023) and Mist (Liang and Wu 2023). Anti-DreamBooth, a variant of AdvDM, incorporates DreamBooth tuning into its optimization process. Mist utilizes a hybrid approach, combining both Encoder (e.g. PhotoGuard) and UNet-based (e.g. AdvDM) protection methods (similar to Eq. 4). We adhere to the hyperparameters specified in their official implementations. Regarding IMPASTO, we employ the same settings used in our application to AdvDM (Section), for both Anti-DreamBooth and Mist. As shown in Table 8, IMPASTO notably enhances the quality of the protected images with comparable protection performances. Figure 13 and 14 also support the efficacy of our method; IMPASTO significantly diminishes visual artifacts in the protected images while preserving the original methods’ style protection ability. These experiments highlight the adaptability and efficacy of IMPASTO across various protection frameworks.

Qualitative results. Figure 15 and 16 provide additional visual comparisons, illustrating the impact of applying IMPASTO in conjunction with PhotoGuard (Salman et al. 2023) and AdvDM (Liang et al. 2023), respectively.

Robustness and generalization. We compare the robustness on countermeasure of IMPASTO in Figure 17, including

JPEG compression, blurring, and noise addition. Across all these countermeasures, IMPASTO demonstrates a protection capability comparable to that of the baseline. In Figure 18, we present additional results demonstrating the generalization capability of IMPASTO. When applied to three different personalization methods—DreamBooth, LoRA, and DreamStyler—IMPASTO maintains performance levels akin to those observed in their respective non-IMPASTO implementations. This highlights the effectiveness and adaptability of IMPASTO across diverse personalization techniques.

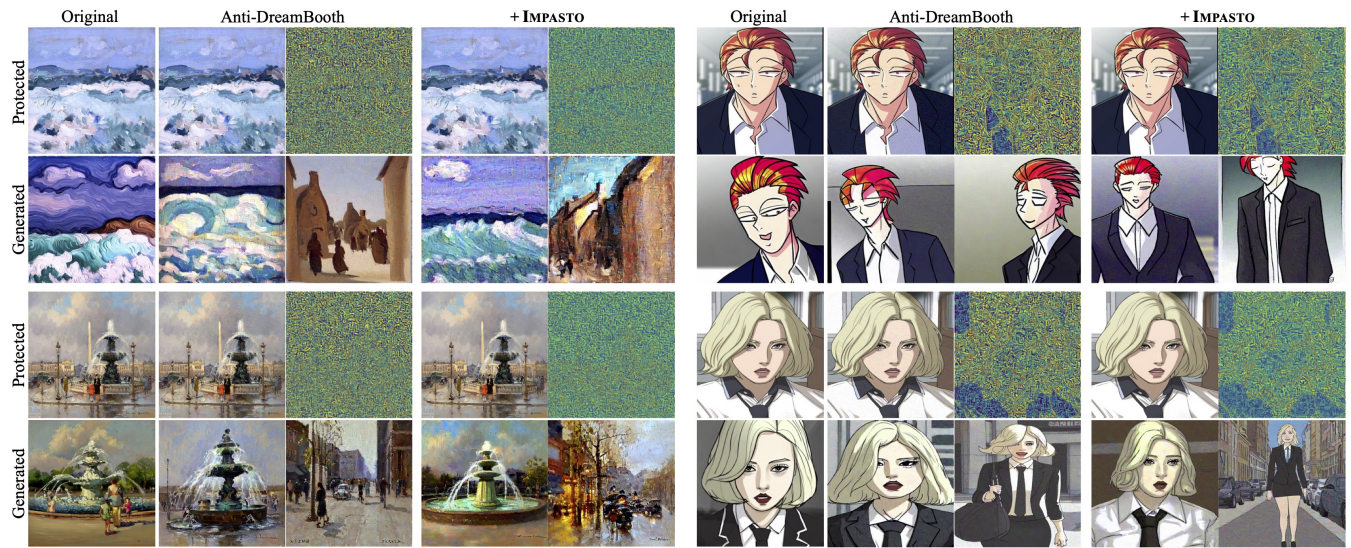


Figure 13: **Qualitative comparison** of Anti-Dreambooth (Van Le et al. 2023) with and without IMPASTO. Best viewed in zoom.

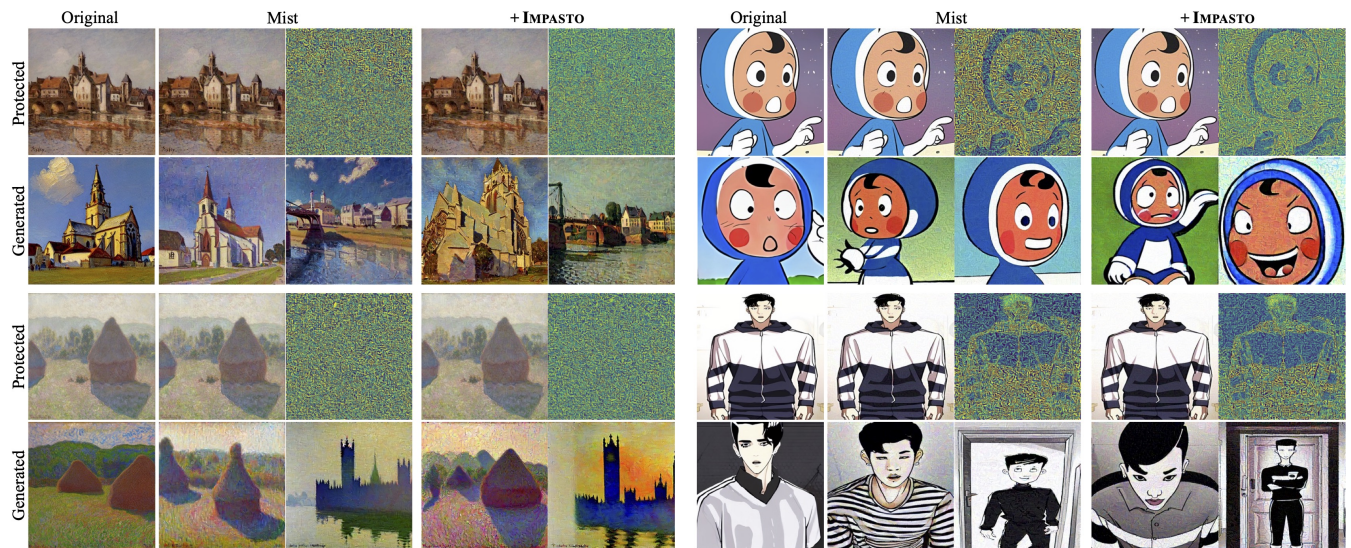


Figure 14: **Qualitative comparison** of Mist (Liang and Wu 2023) with and without IMPASTO. Best viewed in zoom.



Figure 15: **Qualitative comparison** of PhotoGuard (Salman et al. 2023) with and without IMPASTO. Best viewed in zoom.



Figure 16: **Qualitative comparison** of AdvDM (Liang et al. 2023) with and without IMPASTO. Best viewed in zoom.

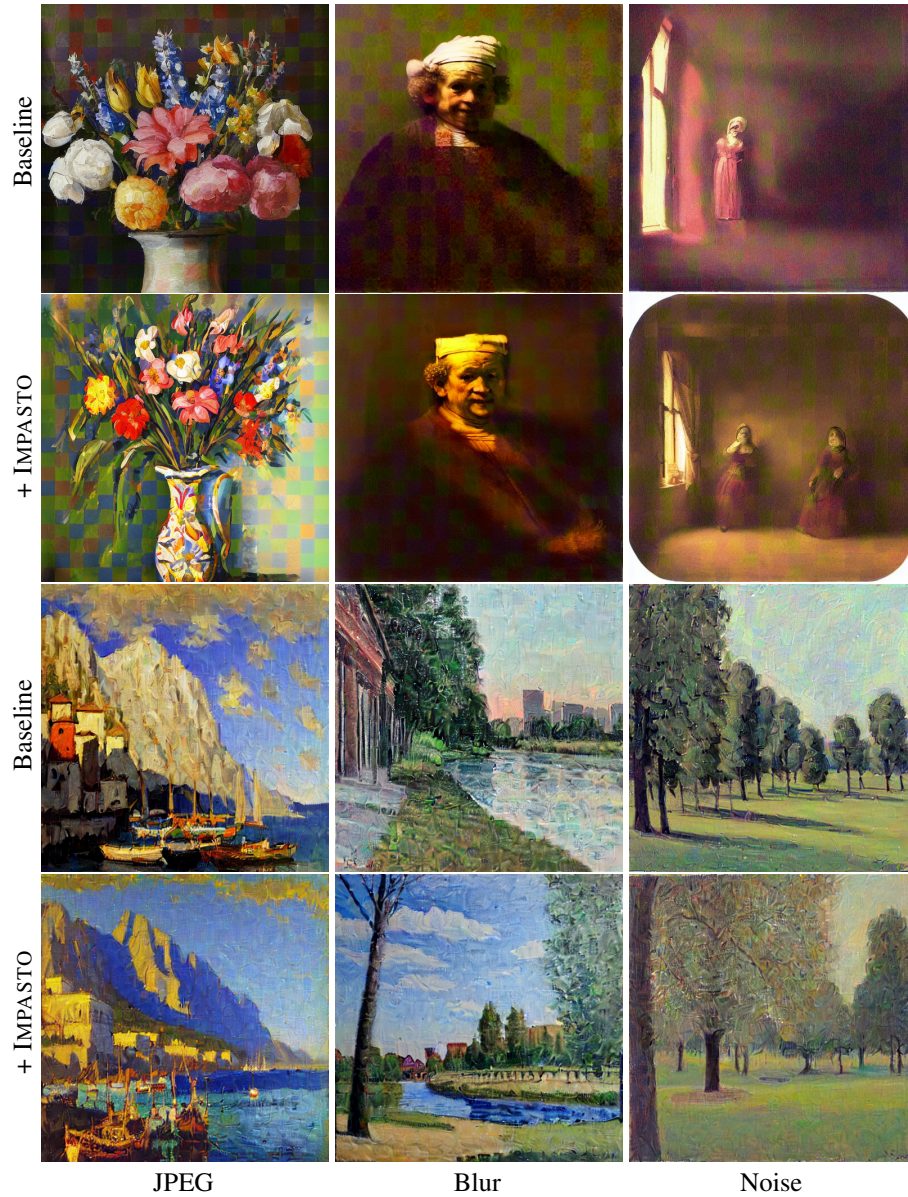


Figure 17: **Qualitative comparison on robustness.** Methods with IMPASTO exhibit comparable protection to the baselines.

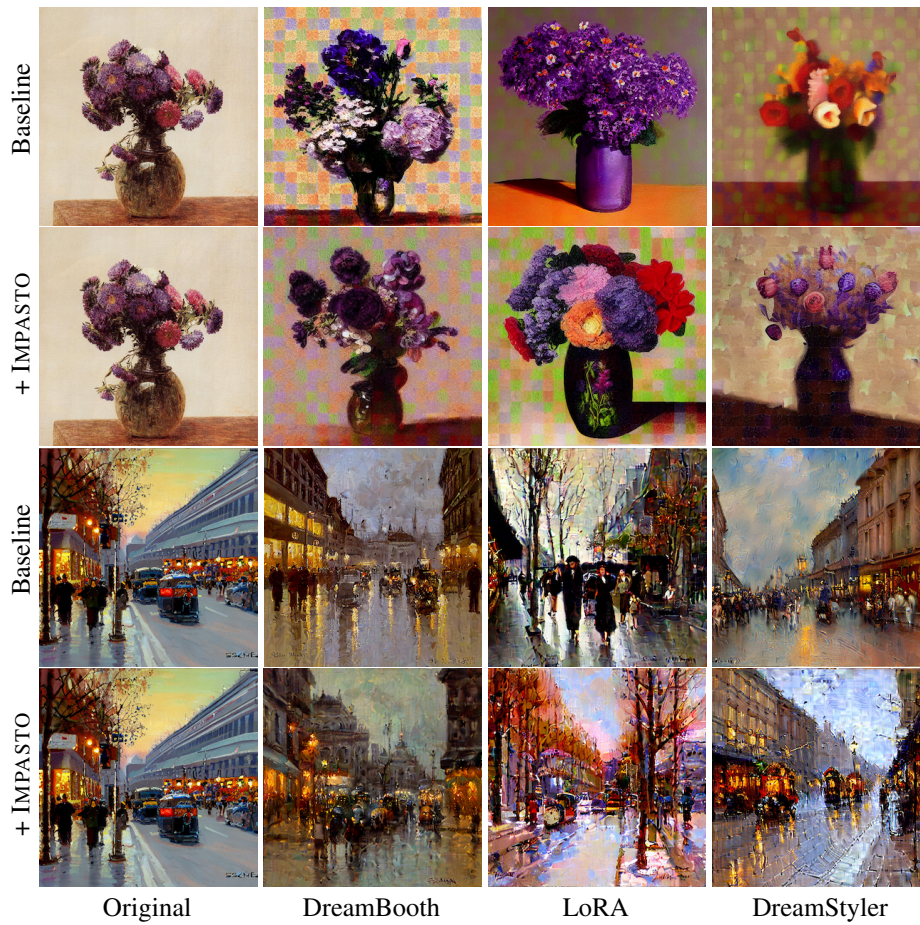


Figure 18: **Qualitative comparison on generalization.** IMPASTO does not impede baseline’s generalization abilities across diverse personalization methods; DreamBooth (Ruiz et al. 2023), LoRA (Hu et al. 2021), and DreamStyler (Ahn et al. 2023)